ACS APPLIED MATERIALS & INTERFACES

Research Article

www.acsami.org

π-Conjugated Polymer Anisotropic Organogel Nanofibrous Assemblies for Thermoresponsive Photonic Switches

Karnati Narasimha and Manickam Jayakannan*

Department of Chemistry, Indian Institute of Science Education and Research (IISER), Dr. Homi Bhabha Road, Pune 411008, Maharashtra, India

Supporting Information

ABSTRACT: The present work demonstrates one of the first examples of π-conjugated photonic switches (or photonic wave plates) based on the tailor-made π-conjugated polymer anisotropic organogel. New semicrystalline segmented π-conjugated polymers are designed with rigid aromatic oligophenylenevinylene π-core and flexible alkyl chain along the polymer backbone. These polymers are found to be self-assembled as semicrystalline or amorphous with respect to the number of carbon atoms in the alkyl units. These semicrystalline polymers produce organogels having nanofibrous morphology of 20 nm thickness with length up to 5 μm. The polymer organogel is aligned in a narrow glass capillary, and this anisotropic gel device is further demonstrated as photonic switches. The glass capillary device behaves as typical λ/4 photonic wave plates upon the illumination of the plane polarized light. The λ/4 photonic switching ability is found to be maximum at θ = 45° angle under the cross polarizers. The orthogonal arrangements of the gel capillaries produce dark and bright spots as on-and-off optical switches. Thermoreversibility of the polymer organogel (also its xerogel) was exploited to construct thermoresponsive photonic switches for the temperature window starting from 25 to 160 °C. The organic photonic switch concept can be adapted to large number of other π-conjugated materials for optical communication and storage.

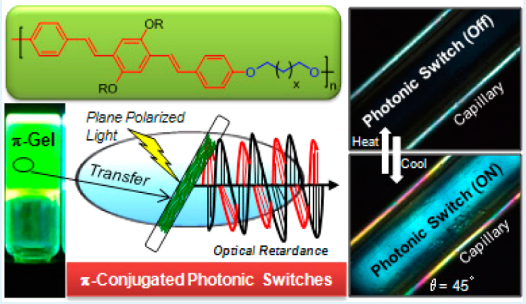

KEYWORDS: *photonic switches, π-conjugated polymers, organogels, semicrystalline polymers, thermoresponsive materials*

INTRODUCTION

Photonic switches (or photonic wave plates) are materials that are capable of transforming the wavelength of light or trafficking optical information for doing specific job or storage.[1−3] Commercial photonic wave plates are made up of silica (quartz) or inorganic crystals, and they are routinely employed as half-wave plates (λ/2) or quarter-wave plates (λ/4) with respect to their function and applications.[4] Owing to the limitation in the processability of the inorganic materials; there is an emerging trend in the last four years for the development of organic photonic switches. Anisotropic supramolecular gels based on oligopeptide assemblies,[5] polypeptide gels,[6] and alginate gels[7] are some of the examples that are recently reported for the above purpose. Photopolymerizable anionic polyterephthalamide hydrogel was also developed for optical sensor applications.[8] Unfortunately, these materials are nonconducting and nonluminescent; thus, they restrict their exploration for photonic switching in tunable optical wavelength and electro-optic devices. π-Conjugated polymers are important classes of materials, and they have both electronic charge mobility as well as tunable absorbance and luminescence properties in the entire visible light and near-IR region.[9] The π-conjugated polymers (or oligomers) are currently extensively tested for applications in photovoltaics,[10] light-emitting diodes,[11] field effective transistors,[12] etc; however, there is no attempt to use π-conjugated materials as photonic switches (or photonic wave plates). For the photonic switching application; it is necessary to choose semicrystalline π-conjugated polymers that would allow the anisotropic alignment of the polymer chains or fibers, which is essential for producing optical retardance[5] with the incident light (see Figure 1). Unfortunately, the chain entanglement in the π-conjugated polymers is a very difficult process to control; consequently, more than 95% of the reported π-conjugated polymers were found to be sluggish to crystallize.[13] Partial alignment of the π-conjugated backbone was achieved by the interdigitations of the alkyl side chains substitution that were primarily introduced for the solubility purpose.[14−16] Unfortunately, these microcrystalline domains (or π-conjugated aggregates) behaved as quenching pockets for diminishing the emission characteristics of π-conjugated core.[17−19] As a result, most often it was rather difficult to find a trade-off between the luminescence properties and crystallinity in π-conjugated polymeric materials for photonic applications.[20]

Segmented π-conjugated polymers based on main-chain substituted analogues is an alternative attractive approach to resolve the above problem. This polymer design provides new opportunity for retaining the photophysical characteristics of

Received: August 15, 2014
Accepted: October 14, 2014
Published: October 14, 2014

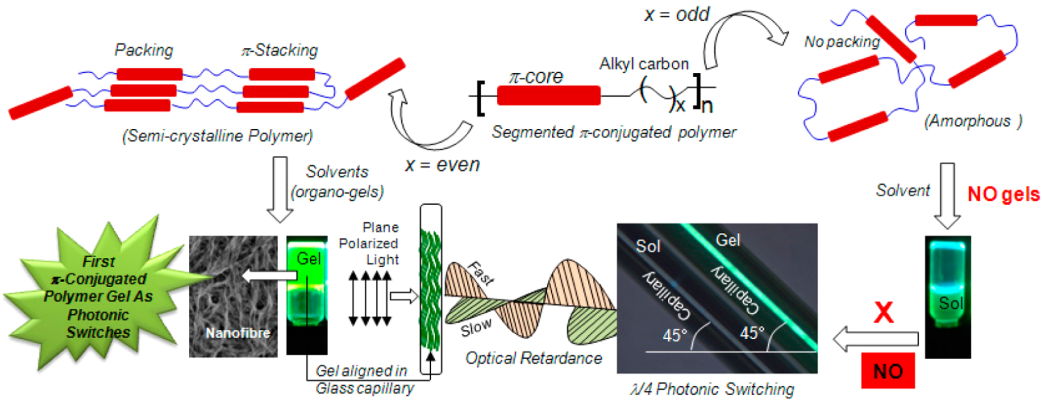

Figure 1. Approaches to develop the first organic photonic switches based on segmented π-conjugated polymer anisotropic organogel.

the π-core and also induces molecular self-assembly along the backbone through chain folding. Karasz and co-workers reported the *p*- and *m*-phenyelenevinylene π-conjugated polymers with polymethylene spacers as light-emitting materials.[21,22] Very recently, Pang and co-workers developed new nanocomposites based on functionalized 1,3-*m*-poly(phenyelenevinylene)s with single-walled carbon nanotubes.[23,24] From our research group, Balamurugan et al. reported carboxylic functionalized segmented π-conjugated polymers and their polymer-Eu^{3+} ions complex as thermosensor as well as chemosensor for metal ions and amino acids.[25,26] Mahima et al. from our group[27] and Ghiggino and co-workers[28] reported independently the donor−acceptor assemblies based on segmented *p*-phenyelenevinylene chromophores with perylenebisimide and C_{60} derivatives, respectively. Unfortunately, these segmented polymers were also found to be amorphous, and they are not suitable for photonic switches. Hence, there is an urgent need to design new semicrystalline segmented π-conjugated polymers for the development of first π-conjugated photonic switches.

The present investigation is emphasized to develop π-photonic switches based on π-conjugated polymer through a molecular self-organization approach (see Figure 1). This concept was based on two important factors: (i) successful development of semicrystalline π-conjugated polymer and (ii) their ability to produce transparent self-organized anisotropic organogel that can be processed into desired objects for testing their photonic switching capabilities. A new segmented π-conjugated polymer strategy was developed in which rigid oligophenylenevinylene (OPV) chromophores were tied in the polymer backbone by flexible alkyl chain bearing carbon atoms 2 to 12. The polymer structures were adopted in such a way that they were devoid of any functional groups (OH, COOH, amide, etc.) and only capable of undergoing self-organization through aromatic π-stacking (or van der Waals forces).[29] On the basis of our previous experience,[27] the structures of the segmented polymers were carefully designed with 2-ethylhexyl units on the OPV core so that complete polymer solubility was achieved for characterization and organogel formation.[30] The present polymer design is unique in that all even-polymers (having even number of alkyl carbons C_n (n = 2,4,...,12) self-organized to produce semicrystalline polymers. Further, the semicrystalline even-analogues self-assembled in organic solvents to produce stable polymer organogels having anisotropic nanofibrous network (see Figure 1). These new semicrystalline anisotropic polymer organogels were loaded and aligned in narrow glass capillaries to make simple optical devices. The capillary devices were demonstrated as photonic switches, more specifically, as λ/4 photonic wave plates. Further, the thermoreversibility of the organogel (or xerogel) was demonstrated as thermoresponsible optical switches for rewritable optical storage in the temperature range of 25−160 °C. Thus, in principle, the organic photonic switches concept demonstrated can be adapted to a large number of π-conjugated polymers to make new optical and electronic devices for future endeavors.

EXPERIMENTAL SECTION

Materials. Hydroquinone, ethylhexyl bromide, triethylphosphite, dibromalkanes, 4-hydroxybenzaldehyde, potassium *tert*-butoxide (1 M in tetrahydrofuran (THF)), and 1-bromodecane were purchased from Aldrich Chemicals. HBr in glacial acetic acid, paraformaldehyde, K_2CO_3, and KOH were purchased locally. Solvents were purchased locally and were purified by standard procedures.

General Procedures. ^1H and ^{13}C NMR were recorded using 400 MHz JEOL NMR spectrometer. Infrared spectra were recorded using a Thermo-Scientific Nicolet 6700 FT-IR spectrometer in solid state in KBr in the range of 4000−600 cm^{-1}. Mass analysis of precursors were determined by the Applied Biosystems 4800 PLUS MALDI TOF/TOF analyzer using TiO_2 as matrix. The molecular weights of polymers were determined using gel permeation chromatography (GPC), which was performed by Viscotek triple detector setup and tetrahydrofuran as solvent. Thermogravimetric analysis (TGA) was done using PerkinElmer STA 6000 simultaneous Thermal Analyzer. Differential scanning calorimetry (DSC) measurements were performed on TA Q20 DSC. The data were recorded at heating and cooling rate of 10 °C/min. The first heating cycle data were discarded since they possessed prehistory of the sample. Powder X-ray diffraction patterns were recorded by Philips Analytical Diffractometer using Cu Kα emission. The spectra were recorded in the range of 2θ = 3−40° and analyzed using X'pert software. Variable-temperature X-ray diffraction studies were performed using a Rigaku Dmax 2500 diffractometer with a copper target. Absorption spectra were recorded using a PerkinElmer Lambda 45 UV spectrophotometer. Steady-state emission and excitation spectra were recorded using Fluorolog HORIBA JOBIN VYON fluorescence spectrophotometer. The solid-state quantum yield was measured using a Model F-3029, Quanta-Phi 6″ Integrating Sphere connected with a Horiba Jobin Yvon Fluorolog 3 spectrophotometer. Field emission scanning electron microscope (FESEM) images were recorded using Zeiss Ultra Plus scanning electron microscope and the samples were prepared by drop casting on silicon wafers and coated with gold. TEM images were recorded using a Technai-300 instrument by drop casting the sample on Formvar-coated copper grid. Atomic force microscope (AFM) images were recorded using Veeco Nanoscope IV instrument. The sample was drop-cast on a freshly cleaved mica surface. The imaging was carried

Scheme 1. Synthesis of Segmented OPV Polymers P-n

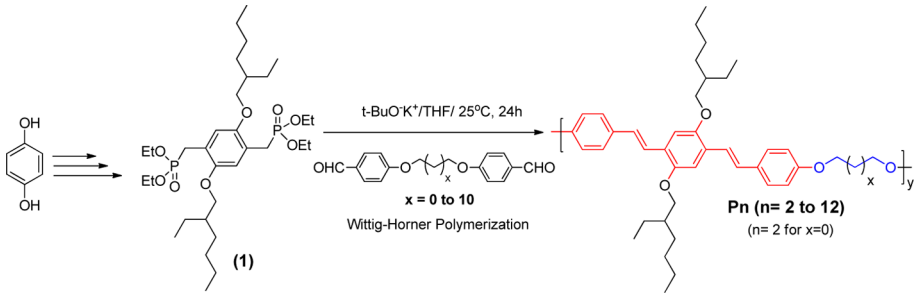

out in tapping mode using TAP-190AL-G50 probe from Budget sensors with a nominal spring constant of 48 N/m and resonance frequency of 163.5. LIECA DM2500 P polarized light microscope equipped with Linkam TMS 94 heating and freezing stage was used. Rheology measurements were done in Anton Paar Physica MCR 301 instrument. A 25 mm parallel plate was used, and measuring system PP08 (d = 0.5 mm) with Peltier control temperature device was used.

Single-Crystal Analysis of OPV-10. For single-crystal X-ray analysis, the good quality crystals were grown in a mixture of chloroform and methanol (1:1 v/v). Crystals were subjected to data collection at 100 K on Bruker APEX duo CCD-X-ray diffractometer equipped with graphite monochromated Mo Kα radiation (λ = 0.710 73 Å). The frames were integrated with Bruker APEX software package. The structures were solved by direct methods and refined with a full matrix least-squares techniques using SHELXS v97 programs. One oxygen and eight carbon atoms of the ethylhexyloxy moiety were disordered. Atom positions of the disordered groups were refined isotropically over two positions using the similar distances and similar U-restraints of the shelx. There is a slightly higher Uiso(max)/Uiso(min) values for the constrained H atoms of the ethylhexyloxy motif owing to the disordered atom positions. The R-factor of the crystal analysis is 8.31%, which is in range acceptable to larger-sized organic crystals.[31,32] The disordered atoms are refined isotropically.

General Procedure for Synthesis of 4,4′-(Alkoxy)-bisbenzaldehyde. The synthesis is described in detail for $\mathbf{C_4}$ spacer, and all other compounds were made following identical procedure. 4-Hydroxybenzaldehyde (6.2 g, 51.0 mmol), 1,4-dibromobutane (2.7 mL, 51.0 mmol), and anhydrous K_2CO_3 (12.7 g, 92.0 mmol) were taken in dry acetonitrile (60.0 mL). The reaction mixture was refluxed for 48 h under nitrogen atmosphere. It was cooled, and the mixture was diluted with dichloromethane (30.0 mL). The solution was filtered, and the solvent was removed under vacuum. Water (50.0 mL) was added to the residue, and the content was extracted with dichloromethane (100.0 mL). The organic layer was dried over anhydrous Na_2SO_4, and the solvent was removed to get product as white solid. The product was further purified by passing through silica gel column using ethyl acetate (18% v/v) in hexane as eluent. Yield = 4.9 g (72%). mp = 107−109 °C. ^{1}H NMR ($CDCl_3$, 400 MHz) δ: 9.89 ppm (s, 2H, C**H**O), 7.85 ppm (d, 2H, **Ar−H**), 7.03 ppm (d, 2H, **Ar−H**), 4.29 ppm (t, 4H, O**CH$_2$**), and 2.36 ppm (m, 2H, C**H$_2$**). ^{13}C NMR ($CDCl_3$, 100 MHz) d: 190.4 (**C**HO), 163.4, 131.7, 129.7, 114.4 (Ar-**C**), 64.2 (O**C**H$_2$) and 28.6 ppm (**C**H$_2$). FT-IR (KBr, cm^{-1}): 2926, 2852, 1675, 1597, 1570, 1500, 1460, 1425, 1387, 1304, 1241, 1206, 1147, 1106, 1035, 960, 822, 731, and 645. MALDI-TOF-TOF-MS (MW = 298.33): m/z = 321.0 (M^+ + 23) and m/z = 337.0 (M^+ + 39).

Detailed procedures for all other compounds having the spacer C_2, C_3, and C_5 to C_{12} are given in the Supporting Information. ^{1}H and ^{13}C NMR data and other details are provided in the Supporting Information

General Procedure for Synthesis of Polymers. All polymers (P-n)s were synthesized using the general method as described for P-4. Monomer (**1**) (0.508 g, 0.8 mmol) and 4,4′-(butane-1,4-diylbis-(oxy))dibenzaldehyde (0.238 g, 0.8 mmol, for polymer P-4) were taken in dry THF (30 mL) and kept under ice condition. Potassium *tert*-butoxide (6.0 mL, 1 M THF solution) was added dropwise to the reaction mixture under a nitrogen atmosphere, and the stirring was continued at 30 °C for 24 h. The resultant yellow-green solution was concentrated and poured into a large amount of methanol. The yellow-green precipitate was filtered and washed with a large amount of methanol. The polymer was dissolved in THF and the solution was filtered and concentrated to 10 mL. The polymer solution was precipitated into methanol to obtain fibrous polymer as product. It was filtered and dried. Yield = 0.312 g. ^{1}H NMR ($CDCl_3$, 400 MHz) δ: 7.47 ppm (d, 4H, **Ar−H**), 7.37 ppm (d, 2H, J = 16 Hz, C**H**=C**H**), 7.11 ppm (s, 2H, **Ar−H**), 7.09 ppm (d, 2H, J = 16 Hz, **CH**=**CH**), 6.91 ppm (d, 4H, **Ar−H**), 4.08 ppm (t, 4H, O**CH$_2$**), 3.95 ppm (d, 4H, O**CH$_2$**), 2.02 ppm (m, 4H, OCH$_2$−C**H$_2$**−C**H$_2$**), 1.82 ppm (m, 2H, OCH$_2$−C**H**−CH$_2$), 1.64−1.38 ppm (m, 18H, **aliphatic-H**), 1.0 ppm (t, 6H, C**H$_3$**), and 0.93 ppm (t, 6H, C**H$_3$**). ^{13}C NMR ($CDCl_3$, 100 MHz) δ: 158.51, 151.0, 130.84, 128.0, 127.61, 126.67, 121.37, 114.65, 110.03, 71.72, 67.50, 39.75, 30.92, 29.25, 26.02, 24.21, 23.11, 14.13, and 11.32 ppm. FT-IR (KBr, cm^{-1}): 3778, 3692, 2922, 2859, 2337, 1600, 1458, 1372, 1338, 1294, 1240, 1173, 1031, 957, 839, 802, 722, and 675.

Detailed procedures for all other segmented polymers having the spacer C_2, C_3, and C_5 to C_{12} are given in the Supporting Information. ^{1}H and ^{13}C NMR, molecular weight data, and other details are provided in the Supporting Information.

By following the above procedure, OPV-10 model compound was also synthesized, and the details are given in the Supporting Information.

RESULTS AND DISCUSSION

Synthesis and Structural Characterization. A homologous series of segmented polymers having rigid oligophenylenevinylene (OPV) aromatic core with different flexible units (C_n, n = 2,3,...,12) along the longitudinal polymer backbone was synthesized as shown in Scheme-1. Hydroquinone was reacted with ethylhexylbromide in the presence of base to give 1,4-bis((2-ethylhexyl)oxy)benzene, which was further reacted with paraformaldehyde and HBr in acetic acid to give corresponding bis-bromomethylated derivative. It was further converted to its corresponding 1,4-bis[(alkyloxy)]-2,5-xylenediphosphonate (**1**). Bis-benzaldehydes were synthesized by reacting 4-hydroxybenzaldehyde with appropriate ω-dibromoalkanes in the presence of potassium carbonate as base in dry acetonitrile. The polymerization of monomer **1** with equimolar amounts of bis-benzaldehydes under Wittig−Horner conditions produced segmented polymers P-n, where n is the number of carbon atoms present in the flexible alkyl chains.

The structures of the polymers were confirmed by ^{1}H NMR, ^{13}C NMR, and FT-IR, and their details are given in the Supporting Information. The ^{1}H NMR spectra of the polymers showed peaks at 7.46 and 6.90 ppm with appropriate splitting pattern corresponding to aromatic phenylene protons (see Figure S1 in the Supporting Information). The two doublets belonging to *trans*-vinylene protons appeared at 7.36 and 7.09 ppm, and the protons in the middle aromatic ring appeared as a

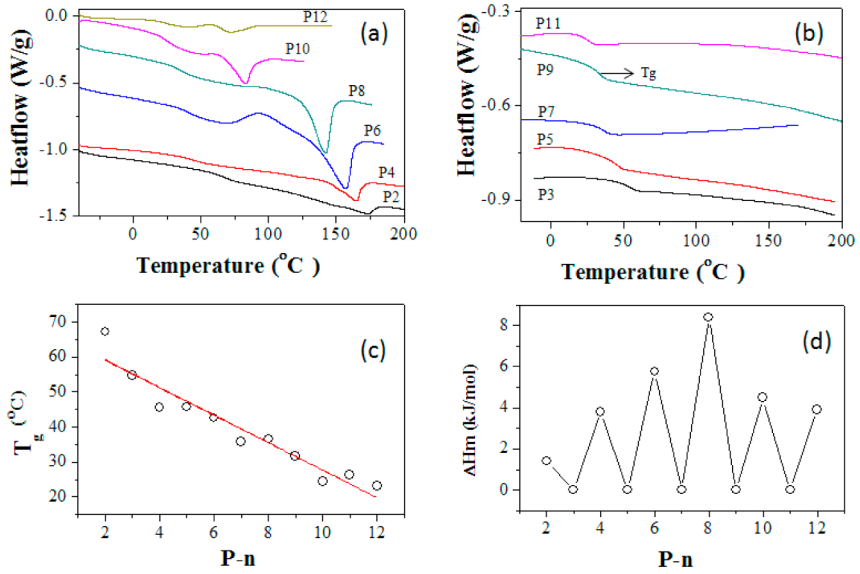

Figure 2. DSC thermograms of the even (a) and odd (b) segmented polymers in the heating cycle 10°/min. (c) Plot of T_g versus the number of carbon atoms in the P-n. (d) Plot of enthalpy of melting versus the number of carbon atoms in the P-n (for odd-segmented polymers, the values are taken as zero due to their amorphous nature).

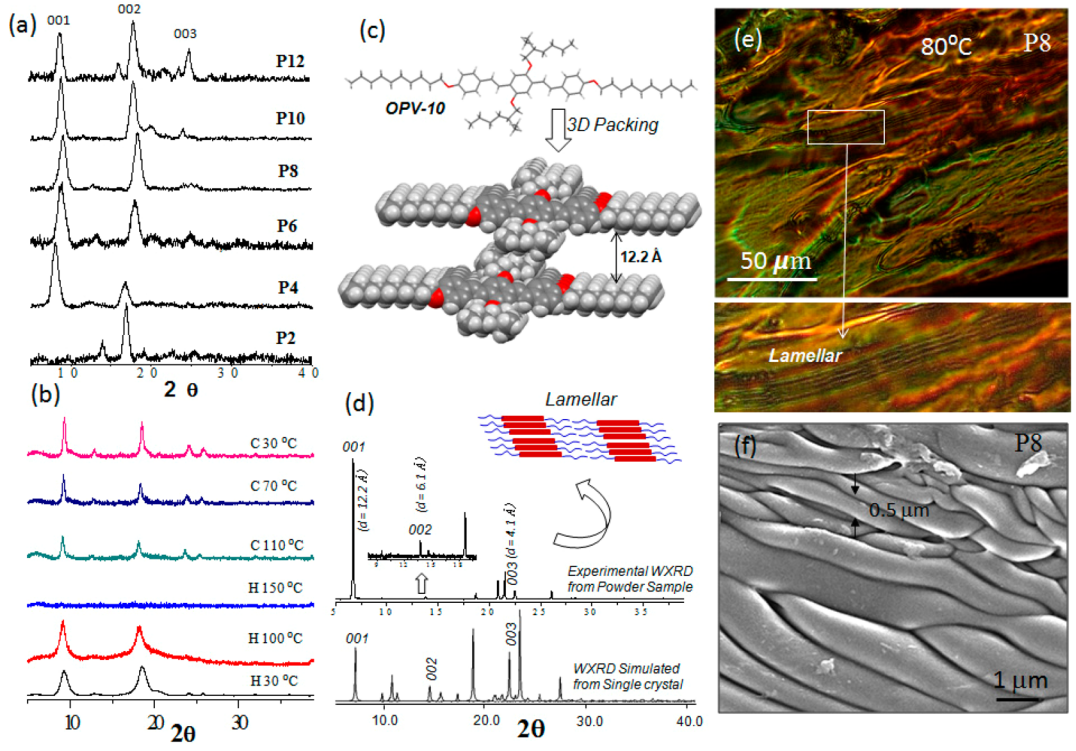

Figure 3. (a) Wide-angle X-ray diffraction pattern for even-polymers P-2 to P-12. (b) Variable-temperature WRXD patterns for P-8 in heating and cooling cycles. (c) Single-crystal structure of oligomer OPV-10. (d) Simulated WXRD pattern for OPV-10 (lower) and its experimental WXRD plot (upper) with assigned Miller indices. (e) PLM image of the P-8 polymer captured on glass substrate at crystallization temperature (80 °C) at 10°/min cooling rate. The expanded PLM images showed the lamellar crystalline domains. (f) FESEM image of P-8 polymer sample on the silicon wafer substrate after crystallization at 10°/min cooling.

singlet at 7.11 ppm. The broad triplets at 4.0 ppm and the doublet in the range of 3.96−3.94 ppm were attributed to Ar-OC**H**$_2$-alkyl and Ar-OC**H**$_2$-EH protons, respectively. The peaks for all other protons appeared below 1.90 ppm. Similarly, ^{13}C NMR spectra of the polymers exhibited aromatic and aliphatic carbons (see Supporting Information, Figure S1).The molecular weights of the polymers were determined by gel permeation chromatography (GPC), and the details are given in Supporting Information (Figure S2 and Table ST1). All the GPC chromatograms appeared as a single peak confirming their monomodel distribution. The molecular weights of the polymers were obtained as M_w = 21 000 to 62 000 g/mol with polydispersities from 1.6 to 4.0 (see Supporting Information, Table ST1). The number-average degrees of

polymerization (n) of the polymers were calculated by dividing their M_n/repeating unit mass (see Supporting Information, Table ST1). These segmented polymers were found to have n = 13 to 25 repeating units indicating that the molecular weights of the polymers obtained were moderate to high. TGA of the polymer confirmed that all the polymers were thermally stable to 350 °C (see Supporting Information, Figure S3).

Odd−Even Effect in Polymer Crystallization. Segmented polymers were analyzed by DSC to trace their thermal properties and solid-state packing. DSC thermograms of the polymers at 10 °C/min heating are shown in Figure 2a,b (see Supporting Information, Figure S4 for their cooling cycles). The segmented polymers with even number of carbon atoms in the alkyl chains (P-n, n = 2, 4, 6, 8, 10, and 12) were found to be semicrystalline, and they showed glass transition (T_g) and melting transitions in the heating cycle (see Figure 2a). In the subsequent cooling cycles, they showed melt crystallization as well as T_g (see Supporting Information, Figure S4). In Figure 2a, both the melting transitions and the T_g values of the polymers decreased with increase in the spacer length. Surprisingly, the segmented polymers with odd number of carbon atoms in the flexible unit (P-n, n = 3, 5, 7, 9, and 11) were found to be amorphous and showed only T_g (see Figure 2b). The plot of T_g versus number of carbon atoms in the alkyl chains revealed that the polymers almost followed a linear trend for the decrease in T_g with increase in the spacer length irrespective of their semicrystalline or amorphous natures (see Figure 2c). The polymer with longer flexible spacer showed low T_g compared to that of the shorter chains. The decrease in T_g was observed as 3.3°/carbon atom in the backbone (see Figure 2c). The semicrystalline and amorphous natures of the segmented polymers were driven by the odd or even number of carbon atoms irrespective of the lengths of spacers (shorter or longer). Enthalpies of the melting transition (ΔH_m) and crystallization (ΔH_c) for the even polymers were determined from DSC thermograms (see Supporting Information, Table ST2). The plot of ΔH_m versus the number of carbon atoms is shown in Figure 2d. The ΔH_m increases with the spacer length and attained maxima at P-8.

This trend indicated that the alkyl chains facilitated the OPV π-core packing at an optimum alkyl spacer length (from P-2 to P-8 polymer). Further increase in the spacer length decreased the chain packing (from P-8 to P-12). A similar trend was observed in the plot of ΔH_c versus the carbon atoms (see Supporting Information, Figure S5). The entropies of the phase transitions were calculated using the following equation:[33] $\Delta S = \Delta H/T$, where ΔH is the enthalpy of the transition at the temperature T (in the Kelvin scale, see Supporting Information, Table ST2 for data). The plot of ΔS versus number of carbon atom (see Supporting Information, Figure S5) showed similar trend as seen in Figure 2d. All the segmented polymers have identical OPV core; thus, the semicrystalline or amorphous nature of the polymers was believed to be driven by the packing of the alkyl chains in the backbone. The polymers with shorter alkyl chains predominantly have large contents of aromatic core; thus, aromatic π-interaction is expected to dictate the solid-state self-assembly.

Segmented Polymer Lamellar Packing. Solid-state packing of the segmented polymers was further investigated by powder wide-angle X-ray diffraction. WXRD patterns of even-polymers P-2 to P-12 are shown in Figure 3a (see Supporting Information, Figure S6 for odd-polymers P-3 to P-11). The even-spacer semicrystalline polymer *P6* showed sharp crystalline peaks at 2 θ = 8.6, 17.93, and 23.2 with respect to order crystalline domains (see Supporting Information, Table ST3). The odd-polymers P-3 to P-11 did not show any diffraction pattern (see Supporting Information, Figure S6), which is indicative of their amorphous nature as observed in their DSC analysis (see Figure 2b). The *d*-spacing of the crystalline peaks in even polymers (for *P4*) were determined as 11.05 Å with respect to first layer of diffractions. Further, these samples did not show any other peaks in the small-angle X-ray diffraction pattern (see Supporting Information, Figure S7); thus, the first peak at 2θ = 8.0 (*d*-spacing 11.05 Å) was assigned to first-order crystalline peak. Variable-temperature WXRD analysis was done for the P-8 to check their thermoreversible packing in the heating and cooling cycles. The variable WXRD patterns of P-8 (see Figure 3b) showed the disappearance of the crystalline peaks at the molten state at 150 °C. In the subsequent cooling, the peaks reappeared, and this trend confirmed their thermoreversible crystallization nature. A similar trend was also observed for polymer *P6* (see Supporting Information, Figure S8). Thus, the even-spacer segmented analogues are very good semicrystalline π-conjugated polymers.

To gain more insight into the packing of crystalline lattices in the WXRD peaks of the segmented polymer, structurally identical OPV oligomer OPV-10 was synthesized (see Scheme SS1 in the Supporting Information). Among the various OPV-n attempted for this purpose, OPV-10 with decyl chain substitution in the longitudinal positions produced good quality crystals in chloroform/methanol. OPV-10 single crystal was resolved, and its structure is shown in Figure 3c. All three aromatic rings occupied the same plane. The molecules were packed in triclinic system, and their unit cell parameters are given in the Supporting Information, Table ST4 and Figure S9. Each OPV-10 molecule was separated apart in the *b*- and *c*-axes equally by 12.7 Å (see Figure 3c). On the basis of our earlier approach,[31,32] powder WXRD for the OPV-10 was computationally simulated from its single-crystal structure, and the Miller indices were assigned in the WXRD pattern (see Figure 3d lower). Powder WXRD pattern for the OPV-10 was recorded experimentally, and it is shown in Figure 3d (upper). The Miller indices for peak in the simulated XRD plot (based on single crystal) matched very well with that of the OPV-10 experimental powder WXRD patterns.[31] The 001 first fundamental peak in the OPV-10 with *d* = 12.2 Å closely matched with the first diffraction pattern at 2θ = 8.0° (*d* = 11.05 Å) in the semicrystalline polymer *P4* (see Figure 3a,b). The 1.1 Å difference between the 001 planes for OPV-10 and *P4* polymer was attributed to the structural difference between the polymer repeating units and OPV-10. Unlike the small OPV molecules, the polymer chains have to undergo chain folding to produce crystalline lattices; thus, the 1.1 Å could account for the polymer crystallization phenomena. This concept was further validated by plotting the *d*-spacing values for 001 peak in the even-segmented polymers (see Supporting Information, Figure S10 and Table ST3). The *d*-spacing decreased from 11.05 to 9.2 Å with increase in the number of carbon atoms from 2 to 12. Thus, the increase in the spacer length was found to slightly decrease the interlayer distance in the lamella. The other two peaks in Figure 3a at $2\theta \approx 18°$ (*d* = 4.9 Å) and $2\theta \approx 24°$ (*d* = 3.57 Å) were assigned to 002 and 003 planes (see Supporting Information, Table ST4).

To visualize the morphology of the lamellar packed semicrystalline polymers, these polymers were further subjected to polarizing light microscope (PLM) and FESEM. In the PLM

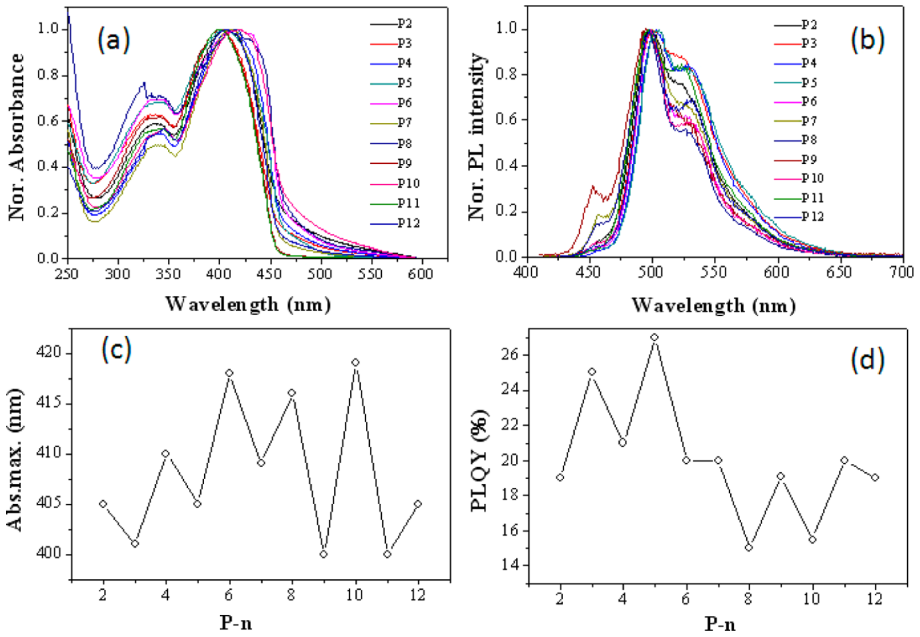

Figure 4. Absorbance (a) and emission (b) spectra of the segmented polymers in thin film. (c) Plots of absorbance maxima vs the number of carbon atoms in the alkyl spacer in P-n. (d) Solid-state photoluminescence quantum yield (PLQY) of the polymers was determined by integrating sphere setup, and these values are plotted against the number of carbon atoms in the alkyl spacer in P-n.

experiment, the polymers were melted and control-cooled at 10°/min using programmed hot stage. PLM images of the polymer P-8 captured during their crystallization process are shown in Figure 3e. The PLM images showed the existence of layered crystalline packing with respect to lamellar-structure. These lamellar structures were reproducible in the repetitive heating and cooling cycles (see more PLM images in Supporting Information, Figure S11). On the other hand, the odd-polymers did not show any crystalline domains; rather, they appeared as glassy solid with respect to their amorphous nature (see Supporting Information, Figure S12). For FESEM imaging (see Figure 3f), the samples were prepared under the identical PLM conditions on the silicon wafer surface at 10°/min cooling from the molten state. The FESEM image of P-8 showed the bundles of submicrometer thick fibers of layered arrangements (see Supporting Information, Figures S13 and S14 for FESEM images of P-4, P-12, and P-5). These thick fibers were entangled with each other as typically observed in thermoplastics. On the basis of the above techniques such as DSC, WXRD, variable-temperature WXRD, single-crystal structure, PLM, and FESEM images; it can be concluded that even-spacer OPV polymers were self-organized as lamellar crystalline solids.

Photophysical Characterization. The photophysical properties of the polymers were studied in solution (toluene) as well as in solid state (in film). In toluene, at dilute concentration, all the polymers showed almost identical absorbance and emission maxima (see Supporting Information, Figure S15). The solution quantum yields of the polymers were determined in the range of 0.3−0.4 using quinine sulfate as standard (ϕ = 0.54 in 0.1 N H_2SO_4,[29] also see Supporting Information, Table ST5).

The absorbance and emission spectra of the polymer thin films are shown in Figure 4a,b. The absorbance maxima of the polymers were plotted against the number of the carbon atoms in the alkyl spacer and are shown in Figure 4c. The overall absorbance of the segmented polymers did not change drastically, and they absorb light in the same range of 400−420 nm. Among them, the even-spacer polymers showed slightly higher absorbance maxima (red-shifted) compared to their neighboring odd-counterparts (typically ±5 to 8 nm). The comparison of the enthalpies of the melting (see Figure 2d) and the absorbance maxima shift (see Figure 4c) revealed that the highly packed polymer chain showed red-shift with respect to strong π-interactions among the OPV chromophores. The plot of the emission maxima versus the number of carbon atoms (see Supporting Information, Figure S16) showed no clear trend for the odd and even spacers. Therefore, absolute solid-state photoluminescence quantum yield (PLQY) was determined using integrating sphere setup to study the role of the lamellar packing on the OPV chromophore emission. The PLQY was done according to the method given by Palsson et al.[34] using the Yvon Horiba Fluorolog-3 instrument. The PLQY of the polymers are shown in Figure 4d. The quantum yields of the polymers varied from 16 to 26% with ±5% with respect to the neighboring counterparts. Interestingly, the odd-polymers showed slightly higher PLQY compared to that of even-polymers. The comparison of the absorbance maxima (see Figure 4c), PLQY (see Figure 4d), and enthalpy of polymers (see Figure 2d) revealed that the strongly packed semicrystalline OPV even-polymers showed slightly less quantum yield compared to the weakly packed odd-polymers (amorphous polymers). This trend is attributed to the luminescence quenching by the crystalline domains that are present in the even-polymers. To further understand the excited-state decay emission dynamics of the polymers, they were subjected to fluorescence lifetime analysis in thin film (see Supporting Information, Figure S17) by time-correlated single photon counting (TCSPC) technique. The polymers were excited with 371 nm light-emitting diode excitation source, and the decay profiles were fitted with DAS 6 program to determine the excitation lifetime. The decay profiles were fitted with biexponential decay, and their decay-rate constants are given in Supporting Information, Table ST6. All the polymers have

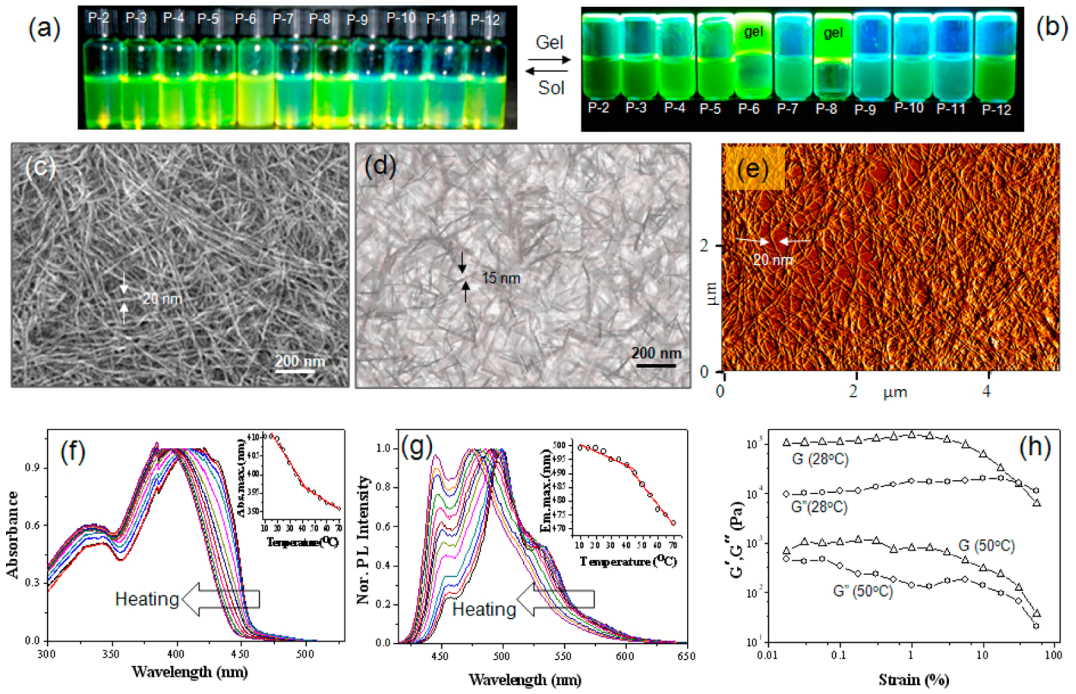

Figure 5. Sol (a) and gel state (b) of the segmented polymers in toluene (10 mg/mL). (c) FESEM, (d) HR-TEM, and (e) AFM images of the P-8 organogel. (f) Variable-temperature absorption and (g) emission spectra of P-8 organogel in toluene. (insets) The plots of absorbance or emission intensity vs temperature. (h) Rheology experimental data of P-8 organogel in the gel (28 °C) and sol state (50 °C).

the decay constants τ_1 = 0.7−1.0 ns and τ_2 = 2.2−3.3 ns, which were comparable to that of reported poly(2-methoxy-5-(2-ethylhexyloxy)-1,4-phenylenevinylene) (MEH-PPV).[17] There is no large difference among the decay excited-state emission dynamics of the segmented polymers irrespective of their semicrystalline or amorphous natures.

Thus, the current polymer design provides the following important observations: (i) the spacer lengths largely influence the packing of the polymer chains, (ii) even-spacer polymer are semicrystalline, (iii) odd-spacer polymer are highly amorphous, and (iv) the odd−even effect induces a small difference in the photophysical characteristics; however, the color of the emission, solid-state quantum yield, and excited-state decay dynamics are almost comparable. This is a very important finding since one can easily tune the semicrystalline or amorphous nature of the polymers without compromising the photophysical characteristics of the π-conjugated system. Unfortunately, the semicrystalline polymers were found to be sluggish to flow in the molten state, which hampered their processability. This was partially associated with the formation of thick submicrometer fibers and also the unavoidable chain entanglement as observed in FESEM images (see Figure 3f). This suggests that alternative methods are required to process π-conjugated semicrystalline polymers into desired objects for loading such as in the narrow glass capillaries for testing their photonic switching capabilities.

Anisotropic π-Conjugated Polymer Gels. Organogels of semicrystalline polymers are important classes of materials, and they preserve the self-organization of the polymer chains in the submicron to nanometer level in the gel state without compromising their processability.[35] A large number of π-conjugated oligophenylenevinylene oligomer-based organogels[36−43] and MEH-PPV polymer organogel[44] have been reported in the literature. The organogel formation ability of the segmented polymers was investigated in a variety of solvents (hexane, dichloromethane, THF, cyclohexane, chloroform, and toluene), and toluene was found to be more suitable for gelation. About 10 mg of the polymer was dissolved in 1 mL of toluene in hot condition, filtered, and subsequently allowed to cool to produce the organogel.

The photographs of the vials containing the polymer in the sol and gel state are shown in Figures 5a,b. All odd-polymers did not self-organize in the solvent, and they did not produce organogel. In the even polymers series, those with low semicrystallinity (P-2, P-4, P-10, and P-12, see Figure 2d) did not produce stable organogels, and only those with high crystallinity, namely, P-6 and P-8, produced organogel. Thus, the present investigation provides direct evidence that the semicrystallinity in the π-conjugated polymer indeed facilitates the formation of stable organogels. The concentrations of the polymers were varied to study their gelation ability, and these results indicated that the polymer P-8 produced more stable organogel (see Supporting Information, Figure S18). The polymer P-6 required large amount of the samples, and the gel was also not stable during the storage; thus, the most stable P-8 organogel was used for the subsequent studies. To visualize morphology of the organogel, the sample was subjected to FESEM, atomic force microscope (AFM), and high-resolution transmission electron microscope (HR-TEM) analysis. FESEM image of the polymer organogel showed the formation of nanofibers of 20 ± 5 nm width and length of up to 5.2 ± 0.4 μm (see Figure 5c). HR-TEM image (see Figure 5d) of organogel confirmed that the size and shape of the nanofibers as observed in the FESEM images. AFM image showed the nanofibrous morphology, and the fibers were found to be helical twist with length up to a few micrometers (see Figure 5e, or more FESEM and AFM images in Supporting Information, Figure S19). The photophyscial and thermal stability of the organogel was investigated by variable-temperature absorbance and fluorescence spectroscopy. The

dx.doi.org/10.1021/am505479z | ACS Appl. Mater. Interfaces 2014, 6, 19385−19396

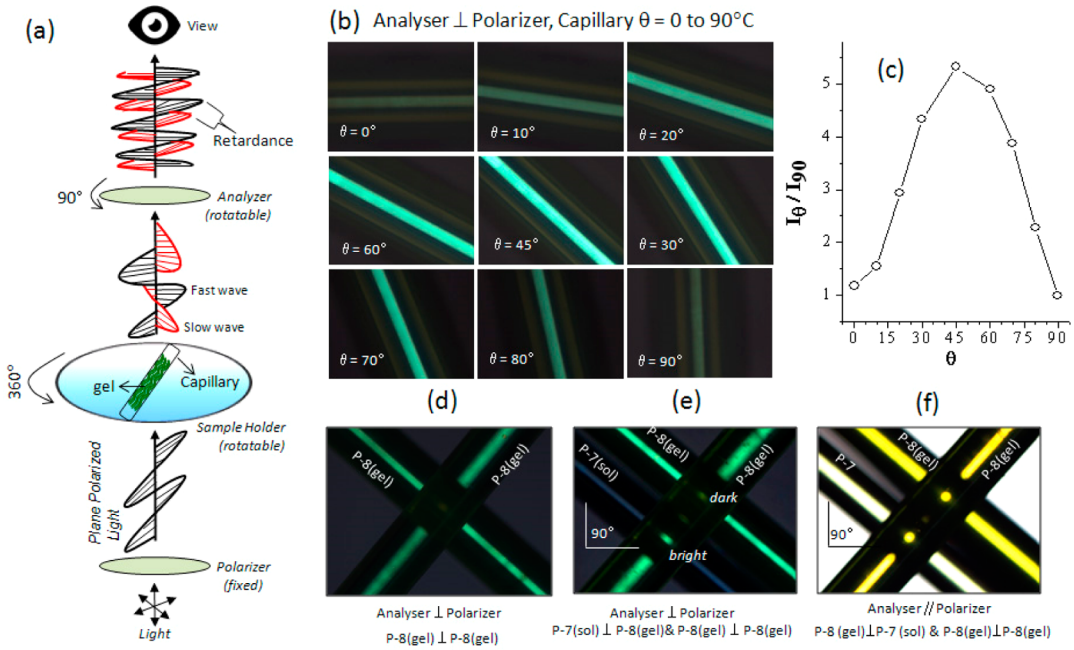

Figure 6. (a) PLM instrument setup used for the studies. The organogel loaded in the glass capillary was placed on the sample holder. (b) Images of the organogel captured at various sample rotation from 0 to 90°. (c) Plot of the intensity of light from the organogel vs the sample rotation θ. (d) Images of the orthogonally aligned glass capillaries of P-8 organogel. (e) Images of P-8 (gel) orthogonal to P-8 (gel) and P-7 (sol) under cross polarizer. (f) Images of P-8 (gel) orthogonal to P-8 (gel) and P-7 under polarizer parallel to analyzer. For all experiments, the angles of the polarizer and analyzer are given along with the images.

absorbance spectra of the gel blue-shifted while heating (see Figure 5f) and red-shifted while cooling (see Supporting Information, Figure S20) with respect to the unlocking and locking of π-aggregation of the OPV chromophore in the polymer backbone, respectively. The emission spectra also showed a similar trend for the reversible aggregation in the heating (see Figure 5g) and cooling cycles (see Supporting Information, Figure S21). The plots of absorbance and emission maxima of the gel versus the temperature (see inset, Figure 5f,g) showed break points at 42−44 °C as gel → sol transition temperature. Mechanical stability of the organogel was studied by dynamic rheological measurement at gel-state (28 °C) and sol-state (50 °C). The plot of dynamic rheological properties of gel is shown in Figure 5h. In the gel state (at 28 °C), the polymers showed 100 times higher values for storage modulus G' and loss modulus G'' at 28 °C compared to that of the sol-state (at 50 °C). Further, both G' and G'' are showed plateau-region with increase in strain as indication of strong network among the nanofibers in the gel state.[45] DSC analysis of the xerogel (see Supporting Information, Figure S22) indicated that the enthalpies of thermal transitions of the xerogel were slightly higher than their semicrystalline polymer. The higher enthalpies were attributed to the better packing of xerogel by the solvent assisted gelation process. The powder XRD analysis of the xerogel (see Supporting Information, Figure S22) showed periodic d-spacing with respect to the layered solid-state ordering as similar to that of semicrystalline sample (see Figure 3a). Photophysical experiments revealed that the P-8 xerogel retained the characteristics of its semicrystalline polymer sample (see Supporting Information, Figure S23). The π-conjugated polymers with even number of carbon atoms in the alkyl spacers have tendency to pack uniformly in the alternative zigzag confirmation to introduce semicrystallinity. On the other hand, the odd number of carbons introduce mismatch for this zigzag arrangement, which produces the amorphous polymer. Thus, this structural diversity in the segmented polymer design makes the even-polymer semicrystalline, whereas the odd-polymer became amorphous (see Figure 1). Further, the higher degree of packing in the even-polymers drove them to aggregate together to produce organogel while cooling the polymer solution from hot toluene. The aligned polymer chains in the organogel produced anisotropic nanofibrous assembly. The amorphous polymer lacks perfect chain alignment and did not produce polymer organogel.

Organic Photonic Switches. Segmented polymer P-8 organogel was transferred into a narrow glass capillary of 1 mm diameter by immersing the capillary into the precooled viscous gel. The gel was uniformly sucked into the tube by capillary action, and by this process polymer chains are aligned unidirectionally along the axis of the cylindrical capillary. The gel was allowed to stay without disturbance for 5 h at 25 °C. The aligned gel was tested for the photonic switching studies using PLM instrument as described in an earlier report,[5] and the details are shown in Figure 6a. The capillary was placed on the sample holder, which can rotate 360°. The instrument has fixed polarizer and an analyzer, which was rotatable 90° at either side of the sample holder. Plane polarized light generated by the polarizer was employed as incident light source for the experiments. Anisotropic soft materials like polymer organogel in the present case refract the plane polarized light differently into slow and fast light waves with right angle to one another. The fast and slow waves emerged from the polarizer showed phase difference, which was observed as optical retardance. Depending upon the nature and the angle at which the sample interacts with the incident plane polarized light, the fast and slow light waves produced either $\lambda/2$ or $\lambda/4$ switching of the incident wave. This phenomenon was traced by keeping the

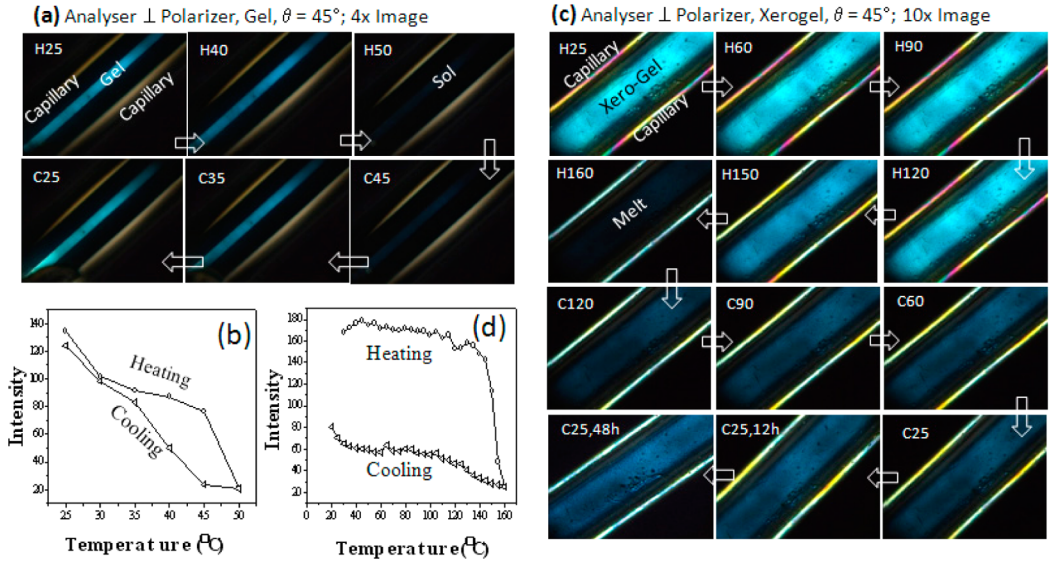

Figure 7. Thermoreversible $\lambda/4$ photonic wave plate behaviors of P-8 organogel (a) and xerogel (c) in the heating and cooling cycles. Plot of the intensity of the organogel (b) and xerogel (d) vs the temperature in the heating and cooling cycles. In the figures, H and C represents heating and cooling cycles, respectively.

analyzer and polarizer perpendicular to each other and rotates the capillary from 0 to 90° in the sample plate (see Figure 6b). When the sample was kept on the same path of the incident plane polarized light (parallel to the polarizer); no light passes through the analyzer (polarizer perpendicular to analyzer). Further, the rotation of the sample from θ = 0 to 45° showed the increase in the intensity of the light from the capillary followed by the interaction of the organogel with incident light. Further increase in the rotation of the sample from θ = 45 to 90° produced the decrease in the intensity of the light from the anisotropic organogel, and the sample became dark at θ = 90°. The intensity of the lights from the sample was measured using imageJ software, and it was plotted against the sample rotation angle, θ (see Figure 6c). This plot clearly indicates that the intensity of the light is maximum at 45° with respect to the typical nature of the $\lambda/4$ type optical switching (or wave plates) of the polymer anisotropic gel.

To further confirm the $\lambda/4$ wave plate behavior of the organogel, the capillaries were subjected to few control experiments as shown in Figure 6d–f. Two P-8 gel capillaries were kept perpendicular to one another and visualized under the cross-polarizers. Interestingly, the point at which the two capillaries cross each other became dark due to the cancellation of the optical retardance of the slow and fast waves from the first capillary to the second one (see Figure 6d). Further, a nongel polymer P-7 solution (in toluene) was filled in glass capillary (no gel formation), and it was placed alongside the P-8 gel capillary. These two parallel capillaries were kept perpendicular to the P-8 gel capillary as shown in Figure 6e. When these capillaries were visualized through the crossed-polarizers, the two P-8 gel capillaries cross-point appeared dark, whereas the P-7 (no-gel) and P-8(gel) cross-point appeared bright. This experiment indicated that two anisotropic gels were required to cancel the optical retardance. The same three capillary arrangements under the illumination of light when the polarizer is parallel to the analyzer did not show the optical retardance (see Figure 6f). These controlled experiments further confirmed that the polymer self-organization into anisotropic organogel is very crucial factor for the $\lambda/4$ wave plate behaviors. Further, the unidimensional alignment of the anisotropic gel in the glass capillary is also a crucial factor for the photonic switching. For instance, the wave plate nature of the organol gel was lost when the gel was spread on two-dimensional glass surfaces (see Supporting Information, Figure S24).

Thermoreversible Optical Switches. The segmented polymer organogel showed thermoreversible self-assembly in the heating and cooling cycles, and these were evident from the studies shown in Figure 5. The combination of the $\lambda/4$ photonic switching and thermoreversible behavior of the anisotropic polymer gel allowed us to develop new thermoresponsive optical wave plates or optical or photonic switches, which may have potential application in the storage and optical transportation of information or sensing that are controllable by heat or thermal behaviors. To demonstrate the above feasibility in the present system, the polymer gel was subjected to variable-temperature photonic switching studies using a temperature-programmable hot stage attached to a polarizing light microscope as shown in Figure 7. The capillary was mounted on the hot stage at θ = 45° and illuminated by plane polarized light under crossed polarizer. The capillary was subjected to control heat or cool at desired temperature. The images captured at the variable temperature above and below the gel melting temperature are shown in Figure 7a. When the capillary was heated from 25 to 50 °C, the intensity of the sample slowly vanished and became dark above the gel temperature point. In the subsequent cooling, the sample has reassembled as anisotropic gel and behaved as $\lambda/4$ wave plates. The plot of temperature versus the intensity of the organogel (Figure 7b) revealed that the intensity of the light was reversible by more than 98% in the heating and cooling cycles. This trend was reproducible in the subsequent heating and cooling conditions. This indicates that the polymer organogel could be used as rewritable optical wave plate depending upon its sol–gel temperature region. To further analyze the thermoreversible nature of the anisotropic gel, the capillary was allowed to dry for 48 h, and the xerogel was subjected to $\lambda/4$ switching studies. DSC analysis of the xerogel indicates that

the sample became molten above 160 °C and aligned back (crystallization) in the subsequent cooling (see Supporting Information, Figure S-22). The images captured at various temperatures of capillary (at θ = 45°) containing the xerogel under crossed polarizers are given in Figure 7c. While heating, the intensity of the emission from the xerogel diminished and became dark at the molten state (at 160 °C). In the subsequent cooling the xerogel reassembled to produce the brightness with $\lambda/4$ behavior. However, the recovery of the intensity became better after annealing the sample at 25 °C for 48 h.

The plot of temperature versus the intensity of the xerogel revealed that ∼30−40% of the self-assembly was reversible (see Figure 7d) in the xerogel state. Thus, the gel is completely reversible for photonic switching in the organogel state; however, the reversibility became very slow in the case of the xerogel. The optical switching by the capillary filled with polymer organogel provides new optical switching possibility up to 160 °C in the neat conditions. Further, semicrystalline polymers are very difficult to fill uniformly in a narrow capillary; however, in the present investigation the ability of the segmented polymer to produce organogel P-8 allow one to fill the narrow capillary devices at the gel state and subsequently remove the solvent to retain the alignment of the crystalline vectors in the xerogel state. The glass capillary device is a simple example developed in the laboratory to demonstrate the proof-of-concept. This photonic switching concept can be expandable to wide range of optical cables with pore size varying from few millimeters to micrometers for optical storage, transmission, or communication. Further, synthetic polymer chemistry provides unlimited opportunity for designing wide variety of π-conjugates with tunable optical band gaps (in the entire visible and near-IR region), electronic configuration (electron rich or deficient), and rigid and flexible backbones; thus, this concept may be explored in other π-conjugates.

CONCLUSION

In conclusion, we have designed new series of semicrystalline segmented π-conjugated polymers with rigid OPV core and flexible alkyl units to demonstrate the first organic photonic switches or organic $\lambda/4$ wave plates. These new classes of segmented polymers were found to be either semicrystalline or amorphous depending upon even or odd numbers of carbon atoms present in the alkyl spacers. Variable-temperature WXRD studies revealed that the polymer chains packed as lamellar network in the solid state. Single-crystal structure of OPV-oligomer was resolved to understand the packing of the lamellar-assemblies in the polymer backbone. Absorbance, emission, solid-state photoluminescence quantum yield, and fluorescence time studies facilitated the understanding of the segmented polymers with respect to even or odd carbon atoms. Interestingly, the even-polymer with highest crystallinity (P-6 and P-8) produced stable polymer organogel unlike their amorphous odd-polymers (no gel formation). The morphology of the P-8 polymer gel was characterized by FESEM, HR-TEM, and AFM analysis. Variable-temperature photophysical studies revealed that the organogel showed thermoreversible sol → gel transition at 42−44 °C. Further, the rheology measurements were carried out to confirm the mechanical stability of the polymer organogel. The organogel was transferred into a glass capillary, and the aligned gel was demonstrated as photonic switches. The polymer organogel was found to behave as $\lambda/4$ wave plates and showed highest intensity for incident plane polarized at θ = 45° under crossed polarizers. The thermoreversibility of the polymer gel was explored to construct thermoresponsive photonic switches for the temperature range from 25 to 160 °C. The optical wave plate concept demonstrated is not restricted to the present segmented OPV polymer design, and it can be adapted to a wide range of other π-conjugated polymers to make futuristic optoelectronic molecular devices.

ASSOCIATED CONTENT

Supporting Information

The synthesis of polymers, OPV-10, structural and molecular weights characterization, TGA and DSC plot, absorption and emission data, FESEM and AFM images, PLM images, variable-temperature XRD, photophysical data, and NMR spectra of the monomers and polymers. This material is available free of charge via the Internet at http://pubs.acs.org. The crystallographic information file (cif) of the single-crystal structure was already deposited to Cambridge Crystallographic data center. CCDC 1013339 contains the supplementary crystallographic data for this paper. These data can be obtained free of charge from the Cambridge Crystallographic Data Centre via www.ccdc.cam.ac.uk/data_request/cif.

AUTHOR INFORMATION

Corresponding Author

*E-mail: jayakannan@iiserpune.ac.in. Fax: +91-20-25908186.

Notes

The authors declare no competing financial interest.

ACKNOWLEDGMENTS

The authors are grateful for the research grant from the Department of Science and Technology (DST), New Delhi, India, under nanomission initiative Project SR/NM/NS-42/2009. We thank MHRD, New Delhi, India, for funding under FAST Scheme. K.N. thanks UGC, New Delhi, India, for research fellowship. We thank Dr. A. Lele, NCL-Pune, for rheology data. We thank Dr. R. Boomishankar and Mr. A. K. Srivastava at IISER-Pune for solving the single-crystal structure.

REFERENCES

(1) Clark, J.; Lanzani, G. Organic Photonics for Communications. *Nat. Photonics* **2010**, *4*, 438−446.

(2) Zhang, C.; Yan, Y.; Yao, J.; Zhao, Y. S. Manipulation of Light Flows in Organic Color-Graded Microstructures towards Integrated Photonics Heterojunction Devices. *Adv. Mater.* **2013**, *25*, 2854−2859.

(3) Benedetto, F. D.; Persano, L.; Cingolani, R.; Pisignano, D.; Mele, E. Multilevel, Room-Temperature Nanoimprint Lithography for Conjugated Polymer-Based Photonics. *Nano Lett.* **2005**, *5*, 1915−1919.

(4) Paschotta, R. *Encyclopedia of Laser Physics and Technology,* Wiley-VCH: Berlin, 2008; Vol. 2

(5) Zhou, J.; Du, X.; Gao, Y.; Shi, J.; Xu, B. Aromatic- Aromatic Interactions Enhance Interfiber Contacts for Enzymatic Formation of a Spontaneously Aligned Supramolecular Hydrogel. *J. Am. Chem. Soc.* **2014**, *136*, 2970−2973.

(6) Zhang, S.; Greenfield, M. A.; Mata, A.; Palmer, L. C.; Bitton, R.; Mantei, J. R.; Aparicio, C.; O.de la Cruz, M.; Stupp, S. I. A Self-Assembly Pathway to Aligned Monodomain Gels. *Nat. Mater.* **2010**, *9*, 594−601.

(7) Maki, Y.; Ito, K.; Hosoya, N.; Yoneyama, C.; Furusawa, K.; Yamamoto, T.; Dobashi, T.; Sugimoto, Y.; Wakabayashi, K. Anisotropic Structure of Calcium-Induced Alginate Gels by Optical and Small-Angle X-ray Scattering Measurements. *Biomacromolecules* **2011**, *12*, 2145−2152.

(8) Wu, Z. L.; Kurokawa, T.; Liang, S.; Furukawa, H.; Gong, J. P. Hydrogels with Cylindrically Symmetric Structure at Macroscopic Scale by Self-Assembly of Semi-Rigid Polyion Complex. *J. Am. Chem. Soc.* **2010**, *132*, 10064−10069.
(9) Kanibolotsky, A. L.; Perepichka, I. F.; Skabara, P. J. Star-Shaped π-Conjugated oligomers and their Applications in Organic electronics and Photonics. *Chem. Soc. Rev.* **2010**, *39*, 2695−2728.
(10) Ye, L.; Zhang, S.; Huo, L.; Zhang, M.; Hou, J. Molecular Design toward Highly Efficient Photovoltaic Polymers Based on Two-Dimensional Conjugated Benzodithiophene. *Acc. Chem. Res.* **2014**, *47*, 1595−1603.
(11) Ying, L.; Ho, C.-L.; Wu, H.; Cao, Y.; Wong, W.-Y. White Polymer Light −Emitting Devices for Solid-State Lighting: Materials, Devices, and Recent Progress. *Adv. Mater.* **2014**, *26*, 2459−2473.
(12) Wang, C.; Dong, H.; Hu, W.; Liu, Y.; Zhu, D. Semiconducting π-Conjugated Systems in Field-Effect Transistors: A Material Odyssey of Organic Electronics. *Chem. Rev.* **2012**, *112*, 2208−2267.
(13) Akcelrud, L. Electroluminescent Polymers. *Prog. Polym. Sci.* **2003**, *28*, 875.
(14) Ren, X.-K.; Wu, Y.-C.; Wang, S.-J.; Jiang, S.-D.; Zheng, J.-F.; yang, S.; Chen, E.-Q.; Wang, C.-W.; Hsu, C.-S. Crystal Structure and Molecular Packing Behavior of Poly(2,3-diphenyl-1,4-phenylenevinylene) Derivatives Containing Alkyl Side-Chains. *Macromolecules* **2013**, *46*, 155−163.
(15) Speros, J. c.; Martinez, H.; Paulsen, B. D.; White, S. P.; Bonifas, A. D.; Goff, P. C.; Frisbie, C. D.; Hillmyer, M. A. Effects of Olefin Content and Alkyl Chain Placement on Optoelectronic and Morphological Properties in Poly(thienylene vinylenes). *Macromolecules* **2013**, *46*, 5184−5194.
(16) Kuo, C-y.; Huang, Y.-C.; Hsiow, C-y.; Yang, Y.-W.; Huang, C.-I.; Rwei, S.-R.; Wang, H.-L.; Wang, L. Effect of Side-Chain Architecture on the Optical and Crystalline Properties of Two- Dimensional Polythiophenes. *Macromolecules* **2013**, *46*, 5985−5997.
(17) Amrutha, S. R.; Jayakannan, M. Probing the π-Stack Induced Molecular Aggregation in π-Conjugated Polymers, Oligomers and Their Blends of Poly(phenylenevinylene)s. *J. Phys. Chem. B* **2008**, *112*, 1119−1129.
(18) Amrutha, S. R.; Jayakannan, M. Structure Control of π-Conjugated Polymers for Enhanced Solid State Luminescence: Synthesis, Liquid Crystalline and Photophysical Properties of New Bulky Poly (p-phenylenevinylene)s and Oligo-Phenylenevinylenes bearing Tricyclodecane Pendants. *Macromolecules* **2007**, *40*, 2380−2391.
(19) Amrutha, S. R.; Jayakannan, M. Control of π-Stacking for Highly Emissive Poly(p-phenylenevinylene)s: Synthesis and Photoluminescence of New Tricyclodecane Substituted Poly(p-phenylenevinylene)s and its Copolymers. *J. Phys. Chem. B* **2006**, *110*, 4083−4091.
(20) Neill, M. O.; Kelly, S. M. Ordered Materials for Organic Electronics and Photonics. *Adv. Mater.* **2011**, *23*, 566−584.
(21) Yang, Z.; Sokolik, I.; Karasz, F. E. A Soluble Blue-light-emitting Polymer. *Macromolecules* **1993**, *26*, 1188−1190.
(22) Pang, Y.; Li, J.; Hu, B.; Karasz, F. E. A Highly Luminescent Poly[(*m*-phenylenevinylene)-*alt*-(*p*-phenylenevinylene)] with Defined Conjugation Length and Improved Solubility. *Macromolecules* **1999**, *32*, 3946−3950.
(23) Chen, Y.; Xu, Y.; Perry, K.; Sokolov, A. P.; More, K.; Pang, Y. Achieving Diameter-Selective Separation of Single-Walled Carbon Nanotubes by Using Polymer Conformation-Confined Helical Cavity. *ACS Macro Lett.* **2012**, *1*, 701−705.
(24) Chen, Y.; Malkovskiy, A.; Wang, X.-Q.; Lebron-Colon, M.; Sokolov, A. P.; Perry, K.; More, K.; Pang, Y. Selection of Single-Walled Carbon Nanotube with Narrow Diameter Distribution by Using a PPE−PPV Copolymer. *ACS Macro Lett.* **2012**, *1*, 246−251.
(25) Balamurugan, A.; Reddy, M. L. P.; Jayakannan, M. π-Conjugated Polymer-Eu^{3+} Complexes: A Versatile Luminescent Molecular probe for Temperature Sensing. *J. Mater.Chem. A* **2013**, *1*, 2256−2266.
(26) Balamurugan, A.; Kumar, V.; Jayakannan, M. Carboxylic Distilbene Fluorescent Polymer Chemosensor for Temperature, Metal-ion and Biomolecule. *Chem. Commun.* **2014**, *50*, 842−845.
(27) Goel, M.; Narasimha, K.; Jayakannan, M. Helical Self-assemblies of Segmented Poly(phenylenevinylene)s and their Hierarchical Donor-Acceptor Complexes. *Macromolecules* **2014**, *47*, 2592−2603.
(28) Tan, T. A. T.; Clarke, T. M.; James, D.; Durrant, J. R.; White, J. M.; Ghiggino, K. P. Synthesis and Photo-induced Charge Separation of Confined Conjugation length Phenylenevinylene Based Polymers. *Polym. Chem.* **2013**, *4*, 5305−5309.
(29) Goel, M.; Jayakannan, M. Supramolecular Liquid Crystalline π-Conjugates: The Role of Aromatic π-stacking and van der Waals Forces on the Molecular Self-assembly of Oligo-Phenylenevinylenes. *J. Phys. Chem. B* **2010**, *114*, 12508−12519.
(30) Segmented polymers were also prepared with methoxy or tricyclodecanemethylene solubilising unit on the OPV core and varying the alkyl chain in the backbone C_2 to C_{12}. The polymers with methoxy substitution were found to insoluble. The tricyclodecanemethylene polymers were found to be soluble only for C_{12} alkyl units (see ref 27). The 2-ethylhexyl substitution is very crucial for complete solubility of segmented polymers in the entire series of C_2 to C_{12} spacers.
(31) Goel, M.; Jayakannan, M. CH/π Interaction Guided Molecular Self-assembly in π-Conjugated Oligomers. *Chem.—Eur. J.* **2012**, *18*, 2867−2874.
(32) Goel, M.; Jayakannan, M. Herringbone and Helical Self-assembly of π-Conjugated Molecules in Solid State through CH/π Hydrogen Bond. *Chem.—Eur. J.* **2012**, *18*, 11987−11993.
(33) Atkins, P. W. *Physical Chemistry,* 6th ed.; Oxford University Press: Oxford, U.K., 1998.
(34) Palsson, L.-O.; Monkma, A. P. Measurements of Solid-State Photoluminescence Quantum Yields of Films Using a Fluorimeter. *Adv. Mater.* **2002**, *14*, 757−758.
(35) Babu, S. S.; Praveen, V. K.; Ajayaghosh, A. Functional π-Gelators and Their Applications. *Chem. Rev.* **2014**, *114*, 1973−2129.
(36) Praveen, V. K.; Ranjith, C.; Bandini, E.; Ajayaghosh, A.; Armaroli, N. Oligo(phenylenevinylene) Hybrids and Selfassemblies: Versatile Materials for Excitation Energy Transfer. *Chem. Soc. Rev.* **2014**, *43*, 4222.
(37) Ajayaghosh, A.; Praveen, V. K. π-Organogels of Self-Assembled *p*-Phenylenevinylenes: Soft Materials with Distinct Size, Shape, and Functions. *Acc. Chem. Res.* **2007**, *40*, 644−656.
(38) Sakakibara, K.; Chithra, P.; Das, B.; Mori, T.; Akada, M.; Labuta, J.; Tsuruoka, T.; Maji, S.; Furumi, S.; Shrestha, L. K.; Hill, J. P.; Acharya, S.; Ariga, K.; Ajayaghosh, A. Aligned 1-D Nanorods of a π-Gelator Exhibit Molecular Orientation and Excitation Energy Transport Different from Entangled Fiber Networks. *J. Am. Chem. Soc.* **2014**, *136*, 8548−8551.
(39) Yao, C.; Lu, Q.; Wang, X.; Wang, F. Reversible Sol−Gel Transition of Oligo(p-phenylenevinylene)s by π−π Stacking and Dissociation. *J. Phys. Chem. B* **2014**, *118*, 4661−4668.
(40) Marciel, A. B.; Tanyeri, M.; Wall, B. D.; Tovar, J. D.; Schroeder, C. M.; Wilson, W. L. Fluidic-Directed Assembly of Aligned Oligopeptides With π -Conjugated Cores. *Adv. Mater.* **2013**, *25*, 6398−6404.
(41) Yagai, S.; Satoru Okamura, S.; Nakano, Y.; Yamauchi1, M.; Kishikawa1, K.; Karatsu, T.; Kitamura1, A.; Ueno, A.; Kuzuhara, D.; Yamada, H.; Seki, T.; Hajime Ito, H. Design Amphiphilic Dipolar π-Systems for Stimuli-responsive Luminescent Materials using Metastable States. *Nat. Commun.* **2014**, *5*, 4013.
(42) George, S. J.; Ajayaghosh, A. Self-Assembled Nanotapes of Oligo(*p*-phenylene vinylene)s: Sol−Gel-Controlled Optical Properties in Fluorescent *p*-Electronic Gels. *Chem.—Eur. J.* **2005**, *11*, 3217−3227.
(43) Ajayaghosh, A.; Praveen, V. K.; Srinivasan, S.; Varghese, R. Quadrupolar p-Gels: Sol−Gel Tunable Red−Green−Blue Emission in Donor−Acceptor type Oligo(*p*-phenylenevinylene)s. *Adv. Mater.* **2007**, *19*, 411−415.
(44) Wang, P. S.; Lu, H. H.; Liu, C. Y.; Chen, S. A. Gel Formation via Physical Cross-Linking in the Soluble Conjugated Polymer, Poly[2-methoxy-5-(2-ethylhexyloxy)-1,4-phenylenevinylene], in Solution by Addition of Alkanes. *Macromolecules* **2008**, *41*, 6500−6504.

(45) Park, J. S.; Jeong, S.; Chang, d. C.; Kim, J. P.; Kim, K.; Park, E.-K.; Song, K.-W. Lithium-induced Supramolecular Hydrogel. *Chem. Commun.* **2011**, *47*, 4736−4738.